Electrochimica Acta 76 (2012) 282–287

Contents lists available at SciVerse ScienceDirect

Electrochimica Acta

journal homepage: www.elsevier.com/locate/electacta

Preparation of metallic cobalt–graphene composites with enhanced electrochemical activity

Lin Wang[a], Dianlong Wang[a,*], Xinchun Hu[a,b], Junsheng Zhu[a], Xiaoshi Liang[a]

[a] *School of Chemical Engineering & Technology, Harbin Institute of Technology, Harbin 150001, China*
[b] *Tian Neng Power International Limited, Wuhu 241000, China*

ARTICLE INFO

Article history:
Received 17 December 2011
Received in revised form 4 May 2012
Accepted 6 May 2012
Available online 14 May 2012

Keywords:
Metallic cobalt
Cobalt hydroxide
Graphene
Hydrothermal reaction
Supercapacitor

ABSTRACT

Metallic cobalt–graphene composites were synthesized through coprecipitation synthetic method followed by hydrothermal treatment at 180 °C. The composite material as prepared was characterized using X-ray diffraction (XRD), SEM, TEM, Energy dispersive spectrometer (EDS) analysis and Thermogravimetric (TG) analysis. The results indicate that metallic cobalt particles possess a good dispersion on the surface of graphene. The electrochemical performance of metallic cobalt–graphene composites was characterized by Cyclic voltammetry (CV) and galvanostatic charge–discharge tests. The specific capacitance of the composite material approaches 1340 F g^{-1} at current density of 1.5 A g^{-1} with a capacitance retention rate of 82% at current density of 3.5 A g^{-1}. The results suggest that the combination of metallic cobalt and graphene leads to synergistic performance, which inherits the overall system with enhanced electrochemical performance.

1. Introduction

Graphene as a rising star has triggered an exciting new area in the field of carbon science, due to its extraordinary electrical [1], chemical stability [2], high surface-to-volume [3] and capacitive performance [4–6]. Moreover, the interleaved network of graphene produces pathways for electron transport, and can obviously improve the electrical conductivity of the electrode. The large surface of graphene provides the platform for the decoration of nanoparticles to avoid their agglomeration, hence more utilization of nanoparticles during the electrochemical reaction. Because of these unique properties of graphene, the combination of graphene with a second phase material can further enhance the electrochemical properties of the obtained composites. Therefore, many materials, including various metal [7], metal oxide nanoparticles [8–11], carbon materials [12], and polymers [13,14], have been used as the second phase to incorporate with graphene. Recently, Lee et al. [15] reported that the specific capacitance of MnO_2–graphene composite electrode was 399.82 F g^{-1} at 10 mV s^{-1}, which demonstrated that graphene layers improved the electro-conductivity of MnO_2 and the interaction between the electrolyte and the electrode. Zhao et al. [16] developed an effective method to prepare monolayer graphene/NiO nanosheets, which indicated that the specific capacitance of the composite was 528 F g^{-1} and much larger than that of pure NiO. Results from Chen et al. [17] shown that the specific capacitance of $Co(OH)_2$–graphene nanocomposite reached a value as high as 972.5 F g^{-1}, which leaded to a significant improvement in relation to each individual counterpart (137.6 and 726.1 F g^{-1} for graphene and $Co(OH)_2$, respectively).

Metallic cobalt has been regarded as a magnetic material [18,19] and several methods have been available for the production of this magnetic material, including physical methods [20], electrochemical methods [21] and chemical methods [22,23]. Herein, to expand the extent of graphene-based composites as electrode materials, we attempted to develop a facile approach to prepare metallic cobalt–graphene composites via coprecipitation synthetic method combined with hydrothermal treatment. The results show that metallic cobalt particles possess a good dispersion on the surface of graphene, which prevents the agglomeration of metallic cobalt particles. The high specific capacitance of the composite material could be expected for the synergistic electrochemical result of the combination of metallic cobalt and graphene in alkaline electrolyte.

2. Experimental

2.1. Preparation of thermal reduced graphene

Thermal reduced graphene (TRG) was prepared from natural graphite powder according to modified Hummers method [24]. 6.5 g of graphite powder was placed in 150 mL of cold (0 °C)

---

[*] Corresponding author at: School of Chemical Engineering and Technology, P.O. Box 411, Harbin Institute of Technology, Harbin 150001, China.
Tel.: +86 451 86413751; fax: +86 451 86413721.
E-mail address: dlwang@hit.edu.cn (D. Wang).

0013-4686/$ – see front matter © 2012 Elsevier Ltd. All rights reserved.
http://dx.doi.org/10.1016/j.electacta.2012.05.022

concentrated H_2SO_4, and then 19.5 g of $KMnO_4$ was added gradually with stirring and cooling, and the temperature of the solution was not allowed to go up to 20 °C. The mixture was stirred at 35 ± 3 °C for 2 h, and 460 mL of distilled water was added slowly to an increase in temperature to 98 °C. The temperature was held at 60 °C for 1 h. Finally, 1.4 L of distilled water and 100 mL of 30% H_2O_2 solution were added after the reaction. The mixture was held at room temperature for 24 h, and then filtered and washed with 5% HCl aqueous solution until sulfate could not be detected with $BaCl_2$. The graphite oxide obtained was dried at 50 °C for 72 h. Thermal reduced graphene was obtained after graphite oxide being put into a muffle oven preheated to 1073 K for 60 s.

2.2. Preparation of metallic cobalt–graphene composites

Metallic cobalt–graphene composites (MCGC) were synthesized through a two-step synthetic method. The typical route was as follows: firstly, 997 mg of cobalt acetate was dissolved in 160 mL of distilled water, and then 27 mg of TRG was dispersed in the above solution with ultrasonication for 1 h. Subsequently, 100 mL of 0.1 mol L^{-1} NaOH aqueous solution was added into the above slurry with vigorous stirring. $Co(OH)_2$–graphene composites (CGC) were collected by filtration, washed with distilled water, and then dried in air at 60 °C.

Then, MCGC were obtained by hydrothermal reaction of CGC with hydrazine hydrate at 180 °C. 70 mg of CGC and 10 mL of 80 wt% hydrazine hydrate were added to 40 mL of distilled water in a Teflon-lined autoclave (85 mL). After stirring of 1 min with a stainless-steel muddler, the autoclave was sealed, and heated at 180 °C for 24 h. The system was then allowed to cool to room temperature. The resulting product was collected by filtration, washed with distilled water, and then dried at 60 °C. For comparison, cobalt hydroxidebare ($Co(OH)_2$) and bare metallic cobalt(BMC) were synthesized via a similar procedure in the absence of graphene.

2.3. Materials characterization

Powder X-ray diffraction (XRD) analysis was performed on Rigaku D/MAX-RC X-ray diffractometer in order to identify the crystalline phases of materials. Morphologies of products as prepared were observed on a field emission scanning electron microscopy(FESEM, Hitachi, S-4800, 15 kV) and a transmission electron microscopy (TEM, Hitachi, H-7650, 100 kV). The element compositions of electrode materials as prepared were determined by an energy dispersive X-ray spectroscopy (EDS, Hitachi, S-4800). Thermogravimetric (TG) analysis was performed using Perkin Elmer Pyris 1 TGA thermo balance. In the TG experiment, the samples were heated in air from 30 to 700 °C at 10 °C min^{-1}.

2.4. Electrochemical measurements

Cyclic voltammetry (CV) curves and galvanostatic charge–discharge tests of electrodes as prepared were investigated under a conventional three-electrode cell with 6 mol L^{-1} KOH aqueous solution as electrolyte at room temperature. The working electrode was fabricated by mixing powders as prepared with 20 wt% acetylene black and 10 wt% polytetrafluorene ethylene (PTFE) binder. A small amount of distilled water was added to the mixture to produce a homogeneous paste. The mixture was pressed onto nickel foam current collectors (1.0 cm × 1.0 cm) to make electrodes. A platinum foil and an Hg/HgO electrode served as counter electrode and reference electrode, respectively. CV curves were collected between −1.3 and −0.2 V (vs. Hg/HgO) and conducted on a CHI 604B electrochemical workstation (Shanghai CH Instrument Company, China). Galvanostatic charge–discharge tests were measured between −1.05 and −0.5 V (vs. Hg/HgO) and investigated by a Neware battery testing workstation.

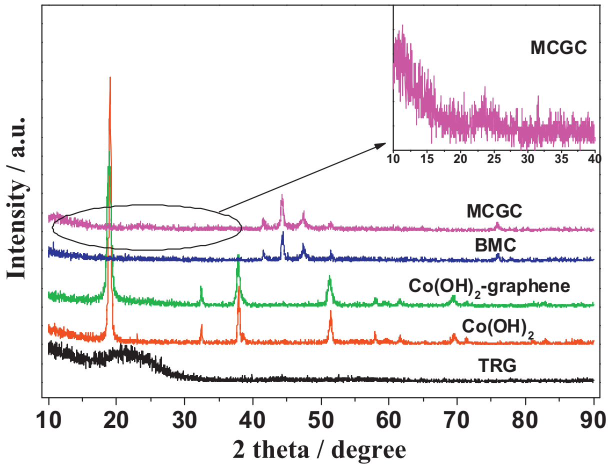

Fig. 1. XRD patterns of the samples as prepared.

3. Results and discussion

The XRD patterns of TRG, $Co(OH)_2$ and BMC extracted from composites, as well as CGC and MCGC are shown in Fig. 1. The diffract peak of TRG at around 21.5° corresponding to 0 0 2 crystal plane of carbon is weak and broad, which indicates that graphene has a highly amorphous nature through thermal treatment. The results of XRD patterns show that diffract peaks of pristine $Co(OH)_2$ as prepared are in good agreement with the standard profile of hexagonal β-$Co(OH)_2$ (JCPDS 30-0443). Moreover, the crystal state of CGC coincides well with that of $Co(OH)_2$. The reflection peak of graphene disappears in the XRD pattern of CGC, which shows that graphene covered by $Co(OH)_2$ is in a state of increasingly disordered stacking. The XRD patterns confirm that BMC consists of hexagonal phase (JCPDS 05-0727) and cubic phase (JCPDS 15-0806). Compared to BMC, a diffraction hump of MCGC appears in the range of 20–27°, which originates for the diffract peak of graphene. This result suggests that the disorderedly stacked structure of graphene tends to an ordered structure through hydrothermal treatment.

The microstructures of TRG, $Co(OH)_2$, BMC, CGC and MCGC are characterized by FESEM in Fig. 2, respectively. The wrinkle and transparent graphene sheets can be seen in Fig. 2(a). Fig. 2(b) shows that the compound $Co(OH)_2$ exists as flat hexagonal platelets in around 300 nm. The FESEM image in Fig. 2(c) reveals that metallic cobalt particles are aggregated together with the particle size of around 400 nm. Fig. 2(d) indicates that $Co(OH)_2$ within CGC is encapsulated in graphene sheets, and CGC possess a layer by layer assembled structure. The FESEM image of MCGC shows that metallic cobalt particles are anchored on the surface of graphene sheets in Fig. 2(e), which prevents metallic cobalt particles from agglomeration. To confirm the elemental composition of MCGC, EDS is employed in Fig. 2(f). The EDS image displays that MCGC consist of cobalt element and carbon element with little of oxygen element which is derived from functional groups on the surface of graphene. The microstructure of MCGC is also observed by TEM in Fig. 3. The TEM image in Fig. 3(a) reveals that metallic cobalt particles possess a good dispersion on the surface of graphene and a maximum particle diameter of 300 nm. Moreover, Fig. 3(b) displays that metallic cobalt particles within MCGC are wrapped by graphene. As will be discussed later, this unique microstructure is beneficial for good accessibility and fast diffusion of the redox phase, which results in the enhanced electrochemical capacitance of the composite material as prepared.

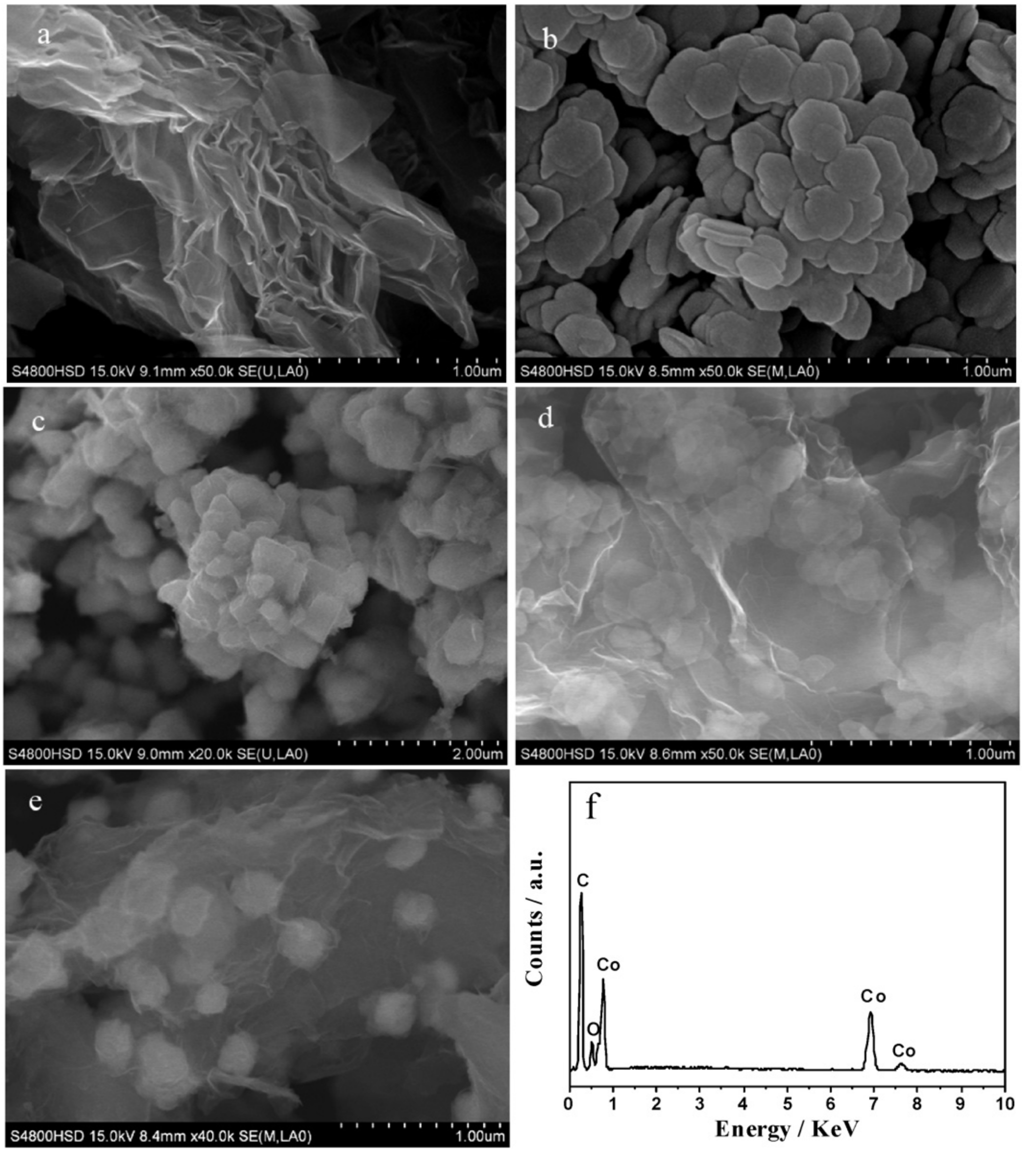

Fig. 2. FESEM micrographs of the samples as prepared: (a) FESEM image of TRG; (b) FESEM image of $Co(OH)_2$; (c) FESEM image of BMC; (d) FESEM image of CGC; (e) FESEM image of MCGC; (f) EDS image of MCGC.

In order to quantify the mass ratio of metallic cobalt to graphene within MCGC, TG curves of TRG, BMC and MCGC are shown in Fig. 4. Normally, some vacancies and topological defects can be simultaneously produced on graphene because of the release of carbon dioxide during thermal treatment. These defect sites lead to the thermal decomposition of graphene at elevated temperature. From this figure, only one step for mass loss of TRG begins at 483 °C with the mass loss of 91.6% [25]. The initial oxidation temperature of

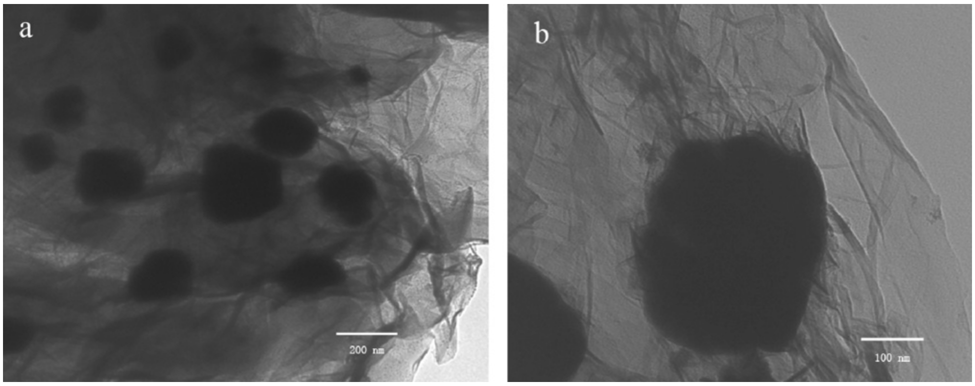

Fig. 3. TEM micrographs of MCGC with (a) low and (b) high magnification.

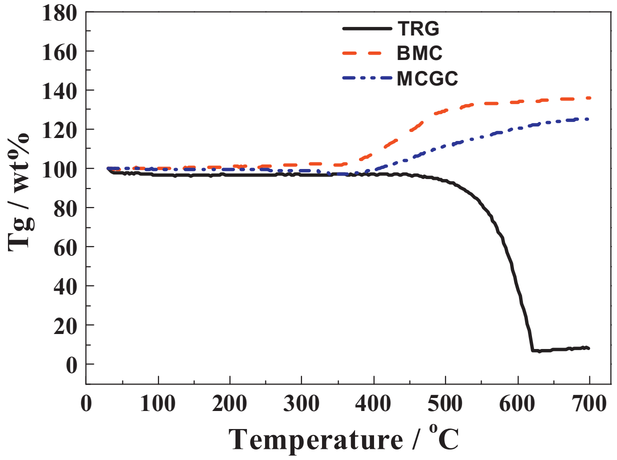

Fig. 4. TG curves of TRG, BMC and MCGC.

metallic cobalt is 343 °C and its residue mass is 136.0% of the original amount. This result indicates that metallic cobalt is completely oxidized to Co_3O_4 while it is exposure to air at this temperature range [26], due to that the molecular weight of Co_3O_4 is 36% higher than that of metallic cobalt. Accordingly, the mass ratio of metallic cobalt to graphene within MCGC can be determined through the TG curve of the composite material. The mass gain behavior of MCGC undergoes a broader temperature range and the mass gain of the composite material is 25.3%, which is assigned to the decomposition of graphene and the generation of Co_3O_4. The mass ratio of metallic cobalt to graphene within MCGC is estimated to be around 8.6:1.

The overall synthetic strategy toward the composite material consisting of metallic cobalt and graphene is outlined in Fig. 5. It is well known that graphene has its basal plane decorated with epoxy and hydroxyl groups, while carboxyl groups are located at the edge. These functional groups, which act as anchor sites, have a high capability of enabling dissolved metal ions to be absorbed on the surface and edge of graphene via electrostatic interaction. Therefore, Co^{2-} ions can be selectively bonded with functional groups through mutual electrostatic attraction. Then, Co^{2-} ions, which are absorbed on the surface of graphene, react with added NaOH to produce $Co(OH)_2$ platelets on the surface of graphene. These platelets are encapsulated in graphene sheets, and increase disorderedly stacked structure of graphene. Through the reduction of CGC in presences of hydrazine hydrate, $Co(OH)_2$ platelets are transformed into metallic cobalt particles which can be firmly attached to the surface of graphene. Moreover, this synthetic methodology is easy and straightforward, therefore can be readily extended as a general procedure to preparation of other metal–graphene nanocomposites.

To explore the potential applications of the composite material as prepared, the samples were fabricated into supercapacitor electrodes and characterized with CV and galvanostatic charge–discharge measurements. Interestingly, the combination of metallic cobalt and graphene enhances electrochemical performance of the whole system. CV curves of TRG, BMC and MCGC at scan rate of $10\,mV\,s^{-1}$ are shown in Fig. 6(a). The loop shape curve of TRG is close to rectangle, which indicates its ideal capacitive performance. A couple of peaks in the CV curve of BMC is observed, which is related to the following redox reaction [27]: $Co(OH)_2 + 2e \leftrightarrow Co + 2OH^-$. The oxidation and reduction peak of metallic cobalt appear at the potential of around −0.696 and −1.072 V, respectively. However, the reduction peak of metallic cobalt is weak in comparison with the oxidation peak, due to slow reduction reaction rate of $Co(OH)_2$ caused by its diffusion process [28]. The CV curve of MCGC shows that the current density of the oxidation peak is obviously enhanced when the oxidation peak migrates to high potential [29]. However, the reduction peak of MCGC is inconspicuous due to that this peak shifts to low potential and is covered by the current of hydrogen evolution reaction. Meanwhile, the reduction current density of the composite material is obviously elevated. The results of CV clearly illustrate that the well-organized interleaved structure consisting of metallic cobalt and graphene facilitates Faraday reaction of metallic cobalt.

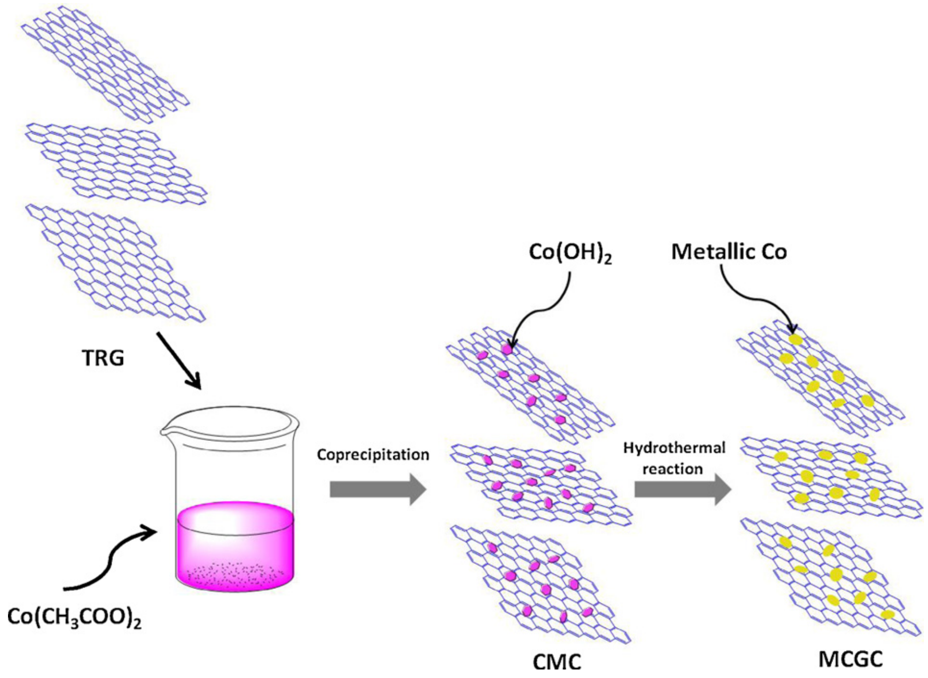

Fig. 5. Synthetic strategy illustration of the composite material consisting of metallic cobalt and graphene.

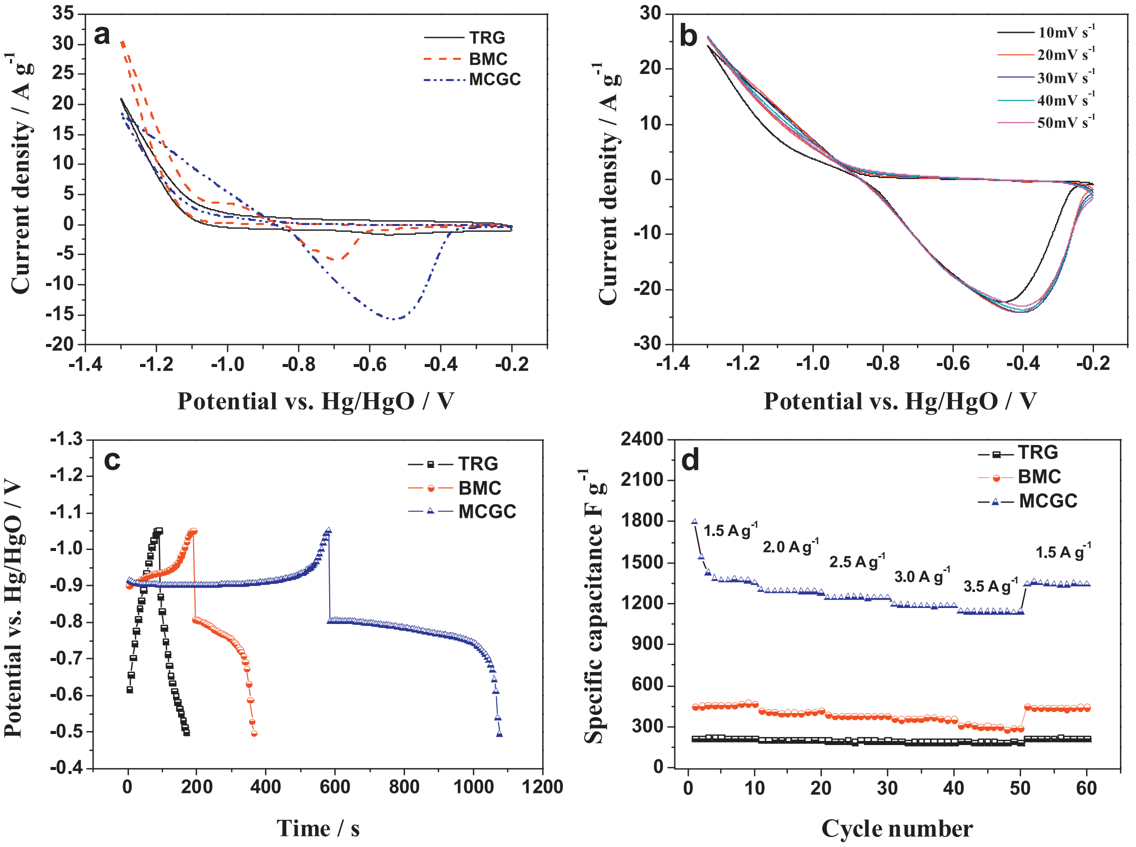

Fig. 6. (a) CV curves of TRG, BMC and MCGC between −1.3 V and −0.2 V (vs. Hg/HgO) in 6 mol L^{-1} KOH aqueous electrolyte; (b) CV curves of MCGC at different scan rates (10 mV s^{-1}, 20 mV s^{-1}, 30 mV, 40 mV s^{-1} and 50 mV s^{-1}); (c) galvanostatic charge–discharge curves of TRG, BMC and MCGC at current density of 1.5 A g^{-1}; (d) rate performance of TRG, BMC and MCGC at different current densities(1.5 A g^{-1}, 2.0 A g^{-1}, 2.5 A g^{-1}, 3.0 A g^{-1} and 3.5 A g^{-1}).

To further explore the electrochemical behavior of MCGC, CV curves of MCGC at different CV scan rates are shown in Fig. 6(b). CV curves of MCGC show that the oxidation current density of MCGC increases with the enhancement of CV scan rate until CV scan rate is increased to 20 mV s^{-1}. However, the oxidation peak current density retains around 25 A g^{-1} as well as the profile of the oxidation peak becomes slightly broad, when CV scan rate proceeds to increase. The results from CV curves of MCGC in Fig. 6(b) suggest that the electrochemical reaction between Co and $Co(OH)_2$ may be controlled by the dissolution–precipitation process of $Co(OH)_2$ rather than the diffusion process of dissolved $Co(OH)_2$ in alkaline solution [28], when CV scan rate is increased adequately.

The comparison of charge–discharge curves of TRG, BMC and MCGC at current density of 1.5 A g^{-1} indicates enhanced electrochemical performance of MCGC in Fig. 6(c). The results obtained from Fig. 6(c) show that the charge–discharge curve of TRG is highly liner and symmetrical, which is a typical characteristic of an ideal capacitive material. MCGC have a longer charge–discharge plateau than BMC, which indicates that MCGC possess a higher capacitance than BMC. In this case, the synergistic effect of the combination of metallic cobalt and graphene on electrochemical performance of the composite material is excellently demonstrated. Graphene is anticipated to serve two roles during the electrochemical reaction. On one hand, graphene prevents the agglomeration of metallic cobalt particles, which can provide unobstructed pathways for ionic transport during the electrochemical reaction. On the other hand, the presence of graphene can contribute to the double-layer which increases the facility of OH^- transportation during the charge–discharge process.

Fig. 6(d) shows specific capacitances of TRG, BMC and MCGC at different current densities. Specific capacitances of the samples are measured according to the following equation [30]:

$$C_s = \frac{I \times \Delta t}{\Delta V \times m} \qquad (1)$$

where C_s is the specific capacitance (F g^{-1}), I is the constant discharge current (A), Δt is the discharge time (s), and ΔV is the potential change during discharge process (V), m is the mass of the active materials in electrode (g). Specific capacitances of TRG, BMC and MCGC are 214 F g^{-1}, 460 F g^{-1} and 1340 F g^{-1} at current density of 1.5 A g^{-1}, respectively. Capacitance retention rates of TRG, BMC and MCGC are 89%, 68% and 82% at current density of 3.5 A g^{-1}, respectively. The results obtained suggest that the three-dimensional network of graphene sheets plays an important role in improving the rate capability of metallic cobalt, due to that metallic cobalt particles are anchored homogeneously on conductive graphene which can promote both the electrochemical utilization of metallic cobalt and the electrical conductivity of the electrode.

As mentioned above, one main reason for the synergistic effect of the combination of metallic cobalt and graphene on electrochemical performance of the composite material is due to that metallic cobalt particles possess a good dispersion on the surface of graphene, which improves the interaction between the electrolyte and the electrode. And the flexible and electrically conductive graphene layers, in which metallic cobalt particles are embedded, can enhance the electrical conductivity of the composite material to reduce the electrochemical polarization of the electrode during the electrochemical reaction. In additional, double-layer capacitive performance of graphene increases the facility of OH^- transportation during the charge–discharge process.

4. Conclusion

In summary, MCGC are prepared through a two-step synthetic methodology. Through the reduction of CGC possessing a layer by layer assembled structure, metallic cobalt particles are firmly attached to the surface of graphene. The specific capacitance of MCGC is $1340\,F\,g^{-1}$ at current density of $1.5\,A\,g^{-1}$ in comparison with the specific capacitance of $460\,F\,g^{-1}$ without graphene. Capacitance retention rates of TRG, BMC and MCGC are 89%, 82% and 68% at current density of $3.5\,A\,g^{-1}$, respectively. As a result, the addition of graphene enhances the storage capacitance and rate capability of metallic cobalt.

Acknowledgment

We gratefully acknowledge the testing support offered by School of Chemical Engineering & Technology, Harbin Institute of Technology.

References

[1] M.D. Stoller, S.J. Park, Y.W. Zhu, J.H. An, R.S. Ruoff, Nano Letters 8 (2008) 3498.
[2] N.R. Wilson, P.A. Pandey, R. Beanland, R.J. Young, I.A. Kinloch, L. Gong, Z. Liu, K. Suenaga, J.P. Rourke, S.J. York, J. Sloan, ACS Nano 3 (2009) 2547.
[3] D.W. Wang, F. Li, Z.S. Wu, W. Ren, H.M. Cheng, Electrochemistry Communications 11 (2009) 1729.
[4] X. Du, P. Guo, H.H. Song, X.H. Chen, Electrochimica Acta 55 (2010) 4812.
[5] Q.L. Du, M.B. Zheng, L.F. Zhang, Y.W. Wang, J.H. Chen, L.P. Xue, W.J. Dai, G.B. Ji, J.M. Cao, Electrochimica Acta 55 (2010) 3897.
[6] Z.Y. Lin, Y. Liu, Y.G. Yao, O.J. Hildreth, Z. Li, K. Moon, C.P. Wong, Journal of Physical Chemistry C 115 (2011) 7120.
[7] L.W. Ji, Z.K. Tan, T. Kuykendall, E.J. An, Y.B. Fu, V. Battagliab, Y.Z. Zhang, Energy & Environmental Science 4 (2011) 3611.
[8] J. Yan, Z.J. Fan, T. Wei, W.Z. Qian, M.L. Zhang, F. Wei, Carbon 48 (2010) 3825.
[9] Y.M. Li, X.J. Lv, J. Lu, J.H. Li, Journal of Physical Chemistry C 114 (2010) 21770.
[10] Y.J. Mai, X.L. Wang, J.Y. Xiang, Y.Q. Qiao, D. Zhang, C.D. Gu, J.P. Tu, Electrochimica Acta 56 (2011) 2306.
[11] Y.L. Chen, Z.A. Hu, Y.Q. Chang, H.W. Wang, Z.Y. Zhang, Y.Y. Yang, H.Y. Wu, Journal of Physical Chemistry C 115 (2011) 2563.
[12] F.C. Meng, X.T. Zhang, B. Xu, S.F. Yue, H. Guo, Y.Z. Luo, Journal of Materials Chemistry 21 (2011) 18537.
[13] K. Zhang, B.T. Ang, L.L. Zhang, X.S. Zhao, J.S. Wu, Journal of Materials Chemistry 21 (2011) 2663.
[14] H.L. Wang, Q.L. Hao, X.J. Yang, L.D. Lu, X. Wang, Nanoscale 2 (2010) 2164.
[15] H. Lee, J. Kang, M.S. Cho, J.B. Choi, Y. Lee, Journal of Materials Chemistry 21 (2011) 18215.
[16] B. Zhao, J.S. Song, P. Liu, W.W. Xu, T. Fang, Z. Jiao, H.J. Zhang, Y. Jiang, Journal of Materials Chemistry 21 (2011) 18792.
[17] S. Chen, J.W. Zhu, X. Wang, Journal of Physical Chemistry C 114 (2010) 11829.
[18] C. Petit, V. Russier, M.P. Pileni, Journal of Physical Chemistry B 107 (2003) 10333.
[19] L.P. Zhu, H.M. Xiao, W.D. Zhang, Y. Yang, S.Y. Fu, Crystal Growth and Design 8 (2008) 1113.
[20] H. Wu, R. Zhang, X. Liu, D. Lin, W. Pan, Chemistry of Materials 19 (2007) 3506.
[21] H. Cao, L. Wang, Y. Qiu, Q. Wu, G. Wang, L. Zhang, X. Liu, ChemPhysChem 7 (2006) 1500.
[22] Q. Xie, Y.T. Qian, S. Zhang, S. Fu, W. Yu, European Journal of Inorganic Chemistry 12 (2006) 2454.
[23] L. Guo, F. Liang, X. Wen, S. Yang, L. He, W. Zheng, C. Chen, Q. Zhong, Advanced Functional Materials 17 (2007) 425.
[24] W.S. Hummers, R.E. Offeman, Journal of the American Chemical Society 80 (1958) 1339.
[25] W.F. Chen, L.F. Yan, P.R. Bangal, The Journal of Physical Chemistry C 114 (2010) 19885.
[26] Z.S. Wu, W.C. Ren, L.B. Gao, J.P. Zhao, Z.P. Chen, B.L. Liu, D.M. Tang, B. Yu, C.B. Jiang, H.M. Cheng, ACS Nano 3 (2009) 411.
[27] P. Elumalai, H.N. Vasan, N. Munichandraiah, Journal of Power Sources 93 (2001) 201.
[28] Y. Han, Y.J. Wang, Y.P. Wang, L.F. Jiao, H.T. Yuan, S.X. Liu, Electrochimica Acta 56 (2011) 3258.
[29] H.M. Du, L.F. Jiao, Q.H. Wang, W.X. Peng, D.W. Song, Y.J. Wang, H.T. Yuan, Journal of Power Sources 196 (2011) 5751.
[30] S.J. Bao, C.M. Li, C.X. Guo, Y. Qiao, Journal of Power Sources 180 (2008) 676.